Performance assessment of a secondary concentrator for solar tower external receivers

Cite as: AIP Conference Proceedings **2126**, 030052 (2019); https://doi.org/10.1063/1.5117564
Published Online: 26 July 2019

Peter Schöttl, Theda Zoschke, Cathy Frantz, Yoel Gilon, Anna Heimsath, and Thomas Fluri

Performance Assessment of a Secondary Concentrator for Solar Tower External Receivers

Peter Schöttl[1, a)], Theda Zoschke[1], Cathy Frantz[2], Yoel Gilon[3], Anna Heimsath[1] and Thomas Fluri[1]

[1]*Fraunhofer Institute for Solar Energy Systems. Heidenhofstr. 2, 79110 Freiburg, Germany.*
[2]*Institute of Solar Research, Aerospace Center (DLR), Pfaffenwaldring 38-40, 70569 Stuttgart, Germany.*
[3]*BrightSource Industries Israel, Ltd, 11 Kiryat Mada St., 91450 Jerusalem, Israel.*

[a)]Corresponding author: peter.schoettl@ise.fraunhofer.de

Abstract. In the EU-project RAISELIFE, a secondary concentrator for Solar Tower systems has been developed conceptually, which is discussed techno-economically herein. Based on a detailed three-level simulation methodology (optical assessment of radiation distribution on receiver surfaces, thermal FEM-simulation of receiver efficiency and transient system simulation), an annual performance assessment of the secondary concentrator by means of a reference system incorporating a receiver with a thermal rating of 600 MW is presented, including a breakdown of the different loss contributions. The annual electrical yield for the secondary setup is increased by 1.57% compared to the reference system, with the potential for further boosts. Regarding material and component costs, an integration of this secondary design could decrease the receiver costs by up to 6.1%.

INTRODUCTION

As part of the EU-funded research project RAISELIFE, several studies have been conducted investigating the design, materials, testing and performance boost of a Solar Tower external receiver with an additional secondary concentrator. This secondary concentrator is designed with an array of trapezoidal flat mirrors which are aligned with the top and bottom edge of each absorber panel. These mirrors allow for intercepting radiation that otherwise wouldn't reach the absorber surface. Therefore, spillage in the system is reduced. In the investigated design, this is exploited by reducing the height of the receiver panels and therefore decreasing the thermal losses and the panel material costs. Furthermore, the secondary protects the equipment above and below the receiver from spilled radiation. This reduces the cost for refractory shields, made from costly high-temperature ceramic materials.
In the following, this secondary is discussed techno-economically.

REFERENCE SYSTEM AND SECONDARY DESIGN

In the scope of the project RAISELIFE, a reference system has been defined whose characteristics follow current market trends. The base case incorporates a 600 MW_{th} molten-salt external receiver on a 200 m tower. The virtual plant is located close to Ouarzazate, Morocco. Measured weather data including DNI and ambient temperature has been used.

For this investigation, the original reference receiver (subsequently referred as *bare receiver case*) has been reduced in height and extended with a secondary concentrator (subsequently referred as *secondary case*). The secondary concentrator is designed with 4-edge-polygonal mirrors, two for each panel. The inclination angles are different for the secondary mirrors at the top and the bottom of the receiver. For details regarding the design of the secondary concentrator, the reader is referred to another SolarPACES 2018 publication [1]. Visualizations of both cases are depicted in Fig. 1.

SolarPACES 2018
AIP Conf. Proc. 2126, 030052-1–030052-8; https://doi.org/10.1063/1.5117564
Published by AIP Publishing. 978-0-7354-1866-0/$30.00

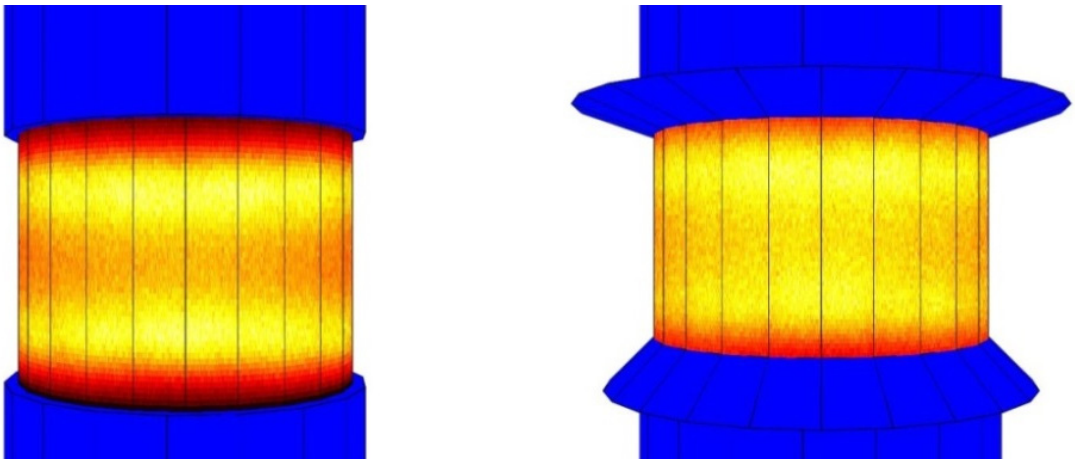

a) b)

FIGURE 1. Reference receiver a) without (bare case) and b) with secondary (secondary case). The top of the panels for both setups is aligned at 200 m. The difference in panel height is clearly visible. On the panels, the flux distribution from ray tracing is visualized. With the secondary, the flux distribution is more homogeneous, particularly at the panel edges and the average concentration is higher.

To simulate realistic solar radiation input for the receiver, a heliostat field with 72000 heliostats has been designed, based on the MUEEN algorithm [2] with several extensions for enhanced flexibility [3]. Circular, excentric field boundaries with a radius of approximately 1200 m have been taken into account according to the reference system definitions (see Fig. 2). The main characteristics of the reference system and both cases are listed in Tab. 1.

TABLE 1. Main characteristics of reference system including bare receiver case and secondary case

Parameter	Value
Number of heliostats	72000
Total mirror area	1497600 m²
Tower height	200 m
Thermal receiver rating	600 MW_{th}
Number of panels	24
Number of tubes per panel	100
Panel width	3.25 m
Panel height bare receiver case	18 m
Panel height secondary case	14.72 m
Thermal storage capacity	2741 MWh_{th}
Power block nominal gross power	150 MW_{el}

SIMULATION METHODOLOGY

To assess the annual performance of the bare receiver and secondary cases, a three-level simulation methodology has been developed, which is outlined in the following.

Optical Ray Tracing Model

An optical model of the heliostat field, the tower structure, the receiver panels and the secondary has been implemented in the tool Raytrace3D [4], which allows for assessing the flux distribution on the absorber surfaces with a high spatial resolution (see Fig. 2). The model yields the absorbed flux on the receiver surfaces and therefore includes reflections from the receiver tubes towards the environment or to other tubes.

The secondary mirrors have been modeled with reflecting polygons, which are attached to the receiver panels at the top and the bottom (see Fig. 1b).

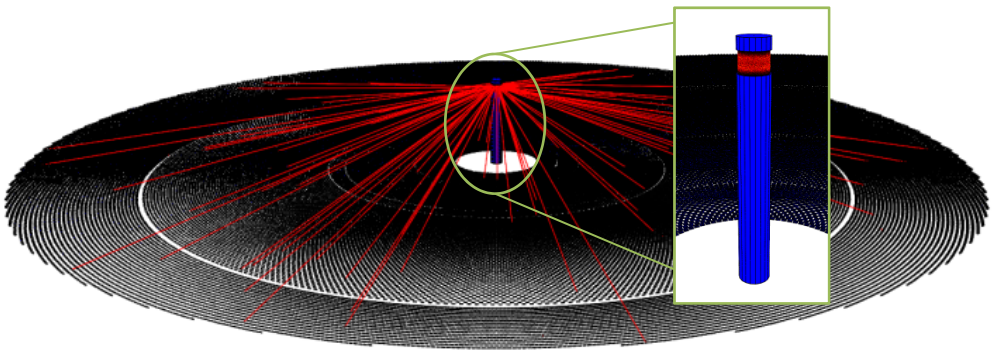

FIGURE 2. Visualization of the ray tracing of the reference system

The optical model takes into account all relevant loss aspects: cosine losses, shading, absorption on heliostats, blocking, spillage, atmospheric attenuation [5] and reflection on the receiver surfaces. The beam spread causing spillage is due to the sun shape (represented with Buie model [6]) and due to mirror slope deviations (represented with Gaussian model).

Mainly due to limitations in the HTF film temperature, the allowable flux density varies depending on the local temperature levels and generally relies on avoidance of flux peaks. For homogenization, an aiming strategy has been applied, which distributes the aim points vertically along the receiver height. The approach is based on the ideas by Binotti et al. [7] and has been extended with circumferentially varying vertical profile functions, that allow for flexibly controlling the flux distributions [2]. For the secondary case, the maximum offsets for the aiming strategy have been extended, which homogenizes the flux on the receiver panels while not increasing the spillage.

As further effort was necessary to comply with the allowable flux density criteria, a defocusing strategy has been implemented [2] which allows for reducing the flux on critical receiver regions.

By using a sky discretization approach with flux map interpolation [2, 8], flux distributions can be readily obtained for any desired sun position and field defocusing state. This has been used to obtain flux maps for several characteristic sun positions and receiver load cases (DNI), which were then input for the thermal receiver model.

Thermal Receiver Model

The thermal losses of the receiver have been simulated using the ASTRID approach [9]. This thermal FEM model considers both the absorber tubes and the insulation. For the computation of the fluid properties, the temperature-dependent correlations published in [10] are used. The local absorbed solar flux as calculated with ray tracing is then applied as a boundary condition on the absorber tubes of the FEM model. The heat transfer to the fluid is modeled using one-dimensional fluid flow elements allowing mass and heat transportation. The local heat transfer coefficients are computed based on Nusselt correlations as a function of the local fluid temperature and Reynolds number based on the Gnielinksi correlation. The thermal radiation exchange between absorber tubes, insulation and ambient is modeled using the radiosity method [11]. The convection losses are simulated by applying a heat transfer coefficient that has been computed for an external receiver without secondary receiver using a CFD model of the receiver [12]. The impact of the secondary concentrator on the convection losses has not been studied; instead it was assumed that the heat transfer coefficient to the ambient is equal for the receiver with and without secondary reflector. Ultimately the model computes the local temperatures of the absorber tubes, insulation and fluid. Based on these temperatures the thermal losses by radiation to the ambient, convection to the ambient and conduction to the ambient are deduced and the thermal receiver efficiency can be calculated based on the following definition:

$$\eta_{\text{therm,rec}} = \frac{P_{\text{absorbed by salt}}}{P_{\text{absorbed solar by receiver}}}$$

$$\text{Absorbed Solar Load factor}_i = \frac{P_{\text{absorbed solar by receiver}}(\text{Load i})}{P_{\text{absorbed solar by receiver}}(\text{Design Point})}$$

Fig. 3 compares the resulting thermal receiver efficiency as a function of the absorbed solar load for a receiver with and a receiver without secondary reflector.

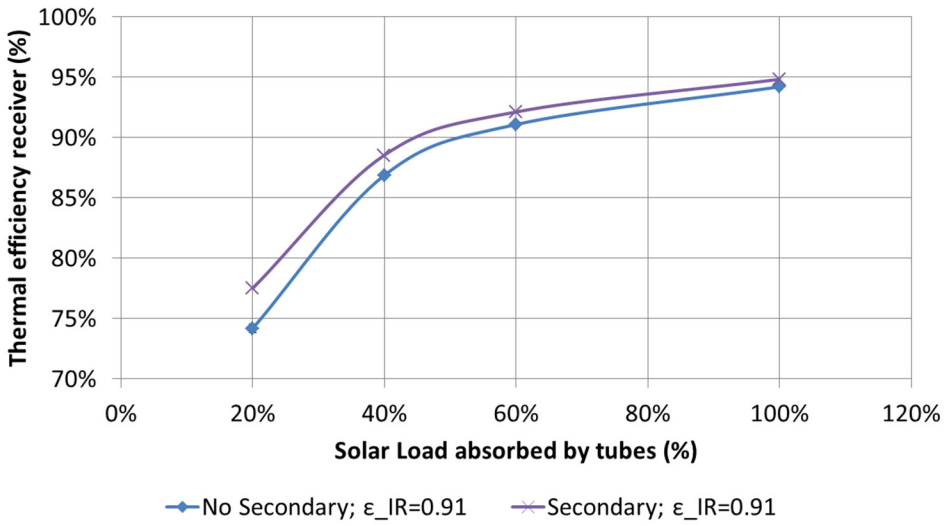

FIGURE 3. Thermal receiver efficiency with and without secondary concentrator as a function of load

The thermal receiver efficiency increases slightly for a receiver with secondary concentrator: for 20% solar absorbed load, the efficiency is increased by 3.3%-point, at design point it is increased by 0.6%-points. The main contributor to the increase in efficiency is the higher solar absorbed mean flux density and hence the lower absorber area of the receiver with secondary receiver, which constitutes 81.8 % of the bare receiver area. At the same time, the higher absorbed solar flux densities lead to an overall increase of the mean absorber surface temperature and hence to higher area specific losses. Indeed the area specific IR-losses to ambient are thereby increased by up to 6.5%, the specific convection losses to 2.7 % for the design point load. For part load cases the temperature-effect decreases because of the lower mean absorber surface temperature resulting from the lower solar flux densities.

For all cases with and without secondary, the maximum molten salt film temperature of 600 °C is not exceeded. Thus, corrosion of the absorber tubes can be avoided.

Annual Yield Simulation

Using the tool ColSim CSP [13], a transient system simulation with a temporal resolution of one minute or less has been used to perform an annual yield assessment. The simulation setup incorporates all relevant components of the reference system: heliostat field and receiver, HTF pump, thermal energy storage and power block (see Fig. 4a). Furthermore, a control strategy has been applied taking into account the technical limitations of the components. Meteorological conditions regarding insolation, wind speed and humidity at the reference site in Morocco are taken into account.

The aforementioned sky discretization approach [8] equally provides optical input for the transient yield simulation, allowing interpolation of flux at each time step without significant additional calculation effort. To obtain the transient thermal efficiency of the receiver, a model has been integrated which interpolates the thermal efficiency from the data generated with the detailed receiver model. Accordingly, the thermal losses can be derived.

A realistic operation strategy is implemented which controls the mass flow rates in the solar field and in the power block according to solar resource availability and storage level respectively. For receiver startup and shutdown, minimum mass flow rate criteria are met guaranteeing that the HTF flow in the receiver is always turbulent. In time periods where either the maximum radiative load on the receiver or the HTF outlet temperature would be exceeded, defocusing of the heliostat field is simulated by limiting the flux. Fig. 4b depicts DNI and thermal receiver yield for two exemplary days in the annual simulation for the bare receiver case. Clearly visible is the delayed startup due to the minimum mass flow criteria and the cut-off where the maximum receiver load is reached.

The model includes pressure losses, which allows calculating the required electrical pumping power as parasitics based on variable pump efficiency.

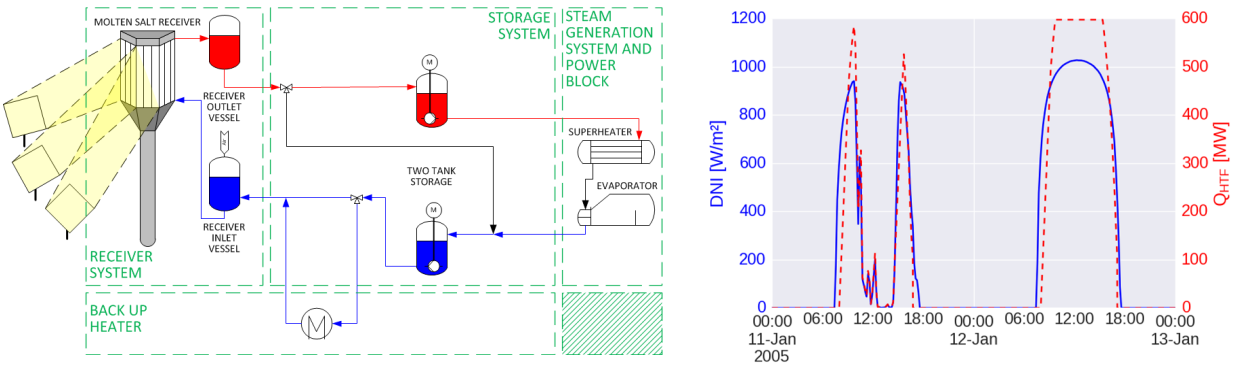

a) b)

FIGURE 4. a) Layout of the reference plant with direct storage integration. b) Exemplary transient DNI and thermal receiver power for two days of the bare receiver reference system

RESULTS AND DISCUSSION

Based on the presented simulation toolchain, the annual yield of both setups has been calculated and compared. The results are also discussed economically. Cost ranges for the secondary mirrors are taken into account.

Loss Breakdown and Annual Gain

Fig. 5 shows a breakdown of losses and gains in the system's energy conversion chain, comparing the bare receiver and secondary cases.

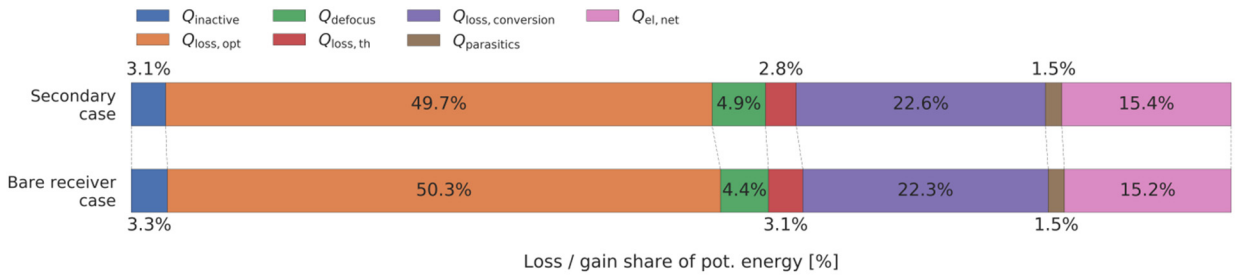

FIGURE 5. For both bare receiver and secondary case, breakdown of losses and gains represented as shares of the potentially available energy $DNI_{annual} \cdot A_{HSF}$. $Q_{inactive}$ includes available DNI when the receiver is not in operation, $Q_{defocus}$ is energy lost to enforced defocusing of heliostats due to maximum receiver power constraints, $Q_{loss,opt}$ are optical losses, $Q_{loss,th}$ are thermal losses, $Q_{loss,conversion}$ are energy conversion losses in the power block and $Q_{parasitics}$ is required pumping power. Annual electrical yield is $Q_{el,net}$.

Annual optical losses are smaller for the system with secondary concentrator, as spillage is reduced. However, a large portion of this is compensated by increased defocusing losses, as the maximum allowable load on the receiver is equal for both systems. Thus, when designing a plant including a secondary concentrator, this aspect has to be taken into account while balancing heliostat field size and receiver load. Either the thermal rating of the receiver should be increased (higher annual yield) or the size of the heliostat field should be reduced (reduction of costs).

The secondary system exhibits smaller thermal losses as the active receiver panels are shorter and the receiver surface area is reduced. The annual average conversion efficiency is 42.7% for both cases, which leads to a relatively higher $Q_{loss,conversion}$ for the secondary case, as more thermal energy is available. With the other loss factors remaining almost unchanged, the integration of the secondary concentrator leads to an increase of annual yield.

For the reference system, annual yields are $Q_{el,net,bare} = 598.5\ GWh$ and $Q_{el,net,sec} = 607.9\ GWh$ for the bare receiver and secondary cases respectively, which implies a relative improvement of the system with secondary by $\frac{Q_{el,net,sec}}{Q_{el,net,bare}} - 100\% = 1.57\%$.

Economic Discussion

To estimate the cost difference between the bare receiver and secondary case, several geometric assumptions were made regarding potential material savings. Furthermore, component and material costs estimations from the RAISELIFE project have been used, which don't include installation and maintenance costs. The cost of the receiver (without tower) is \$30M, which accounts for 7.5% of the total plant costs.

Absorber panels:

- The absorber panel costs are estimated as $C_{panel,bare} = \$10M$.
- For the secondary case with reduced absorber area, the panel costs are scaled linearly with their height: $\frac{C_{panel,sec}}{C_{panel,bare}} = \frac{14.72m}{18m} = 82\%$. This yields cost savings $\Delta C_{panel} = C_{panel,bare} - C_{panel,sec} = \$1.8M$.

Heat shields:

- The rather expensive heat shield material surrounding the receiver at the top and bottom is estimated to be in the range of specific costs $C_{shield,spec} = \$1100/m^2$ ... $\$1600/m^2$.
- By adding the secondary, some of the heat shield material above the receiver can be omitted, as the secondary is effectively protecting the surfaces in its shadow. To calculate the area shadowed by the secondary reflector, the beam projection from the heliostats furthest away is considered. This area is calculated as $\Delta A_{shield} = 217\ m^2$. This yields cost savings $\Delta C_{shields} = C_{shields,bare} - C_{shields,sec} = \Delta A_{shield} \cdot C_{shield,spec} = \$0.239M \ldots \$0.347M$.

Secondary concentrator:

- For the sputtering deposition process of the secondary mirrors, a range of specific costs $C_{mirror,spec} = €10/m^2 \ldots €100/m^2 = \$11.6/m^2 \ldots \$116/m^2$ is projected, with the higher price referring to small production quantities.
- For the truss support, $m_{truss} = 80\ t$ of stainless steel are required. The metal sheets of the mirrors and the stiffening structure would need a thickness $t_{sheet} = 1\ mm \ldots 2\ mm$, which accounts for $m_{sheet} = 50\ t \ldots 100\ t$ of stainless steel.
- The specific stainless steel costs are estimated as $C_{steel,spec} = €2/kg = \$2.32/kg$, with an exchange rate $€/\$ = 1.16$.
- With a total secondary mirror area of $A_{sec} = 1021.4m^2$, this yields a range of secondary costs $C_{sec} = A_{sec} \cdot C_{mirror,spec} + (m_{truss} + m_{sheet}) \cdot C_{steel,spec} = \$0.313M \ldots \$0.536M$.

Based on these cost projections, the cost difference between bare receiver and secondary setups is estimated as

$$\Delta C_{rec,sec} = C_{sec} - \Delta C_{shields} - \Delta C_{panel} = -(\$1.50M \ldots \$1.83M)$$

for the worst (lowest savings regarding shield costs, highest secondary mirror costs) and best case respectively.
Thus, the costs of the secondary setup are lower as compared to the bare receiver setup, which accounts for 5.0% ... 6.1% of the receiver costs.

Due to a lack of detailed and accurate cost information in the conceptual phase, the economic discussion remains rather superficial. Other additional costs of the secondary might arise which are not discussed here. In particular, no information about additional installation and maintenance costs is included, with the latter being due to required cleaning of the secondary mirrors. Furthermore, the availability of secondary mirrors able to withstand the high temperatures is yet unclear. Their development is part of the aforementioned RAISELIFE project. In case, the mirrors degrade over time, additional replacements costs would be implied. If required, an active cooling system would lead to additional investment costs and auxiliary energy consumption.

Despite the lack of detailed cost information, the discussion provides an indication that the integration of secondary concentrators can be economically beneficial even regardless of any increases in yield.

CONCLUSION

A performance assessment for a secondary concentrator for Solar Tower plants with external receivers – as developed in the project RAISELIFE – has been presented. For the technical assessment of the secondary, a three-level simulation model has been implemented, incorporating transient optical assessment of heliostat field and receiver, detailed FEM evaluation of the thermal receiver efficiency and annual yield assessment of the entire plant. Differences in thermal efficiency strongly depend on the transient receiver load, which highlights the importance of annual performance assessment.

Simulations show reductions regarding optical as well as thermal losses, which lead to 1.57% increased electrical yield. As a share of the benefits of the secondary concentrator is compensated by increased defocusing losses, an even higher boost of the yield could be reached by carefully re-designing the secondary system. Economically, the system is discussed based on assumptions regarding material savings and specific costs. With the integration of the secondary, cost savings in the range of $\$1.50M \dots \$1.83M$ are possible, mainly due to the reduction of panel height. This accounts for $5.0\% \dots 6.1\%$ of the receiver costs.

Based on the technical assessment and the cost calculations, the investigated system can be considered beneficial both economically and regarding the yield, as compared to the bare receiver reference. However, many open questions regarding the implementation of a secondary concentrator in practice are out of scope of this study, but will be dealt with in future work.

ACKNOWLEDGMENTS

This project has received funding from the European Union's Horizon 2020 research and innovation programme under grant agreement No 686008 (RAISELIFE).

REFERENCES

1. R. Uhlig, J. Hertel, C. Frantz, and Y. Gilon, "Thermal Analysis and Design of a Secondary Concentrator for External Molten Salt Receivers," submitted to 24th SolarPACES Conference, 2 – 5 October 2018, Casablanca, Morocco.
2. P. Schöttl *et al.,* "Efficient modeling of variable solar flux distribution on Solar Tower receivers by interpolation of few discrete representations," *Sol Energy*, vol. 160, pp. 43–55, 2018.
3. E. Leonardi *et al.,* "Techno-Economic Heliostat Field Optimization: Comparative Analysis of Different Layouts," *Submitted to Solar Energy Journal*, 2018.
4. R. Branke and A. Heimsath, "Raytrace3D-Power Tower - A Novel Optical Model For Central Receiver Systems," in *SolarPACES 2010*.
5. P. L. Leary and J. D. Hankins, "User's guide for MIRVAL: A computer code for comparing designs of heliostat-receiver optics for central receiver solar power plants," Laboratories, Sandia, Livermore, CA SAND-77-8280 United StatesThu Feb 07 21:28:27 EST 2008Dep. NTIS, PC E04/MF E04.SNL; ERA-04-032944; EDB-79-054524English, 1979.
6. D. Buie, A. G. Monger, and C. J. Dey, "Sunshape distributions for terrestrial solar simulations," (English), *Sol Energy*, vol. 74, no. 2, pp. 113–122, 2003.
7. M. Binotti, P. de Giorgi, D. Sanchez, and G. Manzolini, "Comparison of Different Strategies for Heliostats Aiming Point in Cavity and External Tower Receivers," *J. Sol. Energy Eng*, vol. 138, no. 2, p. 21008, 2016.
8. P. Schöttl, K. Ordóñez Moreno, F. C. D. van Rooyen, G. Bern, and P. Nitz, "Novel sky discretization method for optical annual assessment of solar tower plants," *Solar Energy*, vol. 138, pp. 36–46, 2016.
9. C. Frantz, A. Fritsch, and R. Uhlig, "ASTRID© – Advanced Solar Tubular ReceIver Design: A powerful tool for receiver design and optimization," in *AIP Conference Proceedings 1850: International Conference on Concentrating Solar Power and Chemical Energy Systems*, Abu Dhabi, United Arab Emirates, 2017.
10. J. E. Pacheco *et al.,* "Final Test and Evaluation Results from the Solar Two Project," Sandia National Laboratories, Albuquerque, NM (United States) SAND2002-0120, 793226, 2002. [Online] Available: http://www.osti.gov/servlets/purl/793226-0lbooq/native/. Accessed on: Oct. 26 2012.
11. SAS IP, Inc., "ANSYS, Inc. Release 17.0 Product help: Chapter 6.5 – Radiosity Solution Method. Release 17.0,"

12. S. Giuliano *et al.,* “HPMS - High Performance Molten Salt Tower Receiver System : öffentlicher Schlussbericht : 01.10.2014-31.12.2016,” HPMS - Entwicklung eines hocheffizienten Receiversystems für Salzturmkraftwerke, Deutsches Zentrum für Luft- und Raumfahrt e.V., Institut für Solarforschung, Stuttgart, 2017.
13. C. Wittwer, “ColSim - Simulation von Regelungssystemen in aktiven solarthermischen Anlagen,” Universität Karlsruhe, Fakultät für Architektur, 1999.